Supplementary material

Phosphodiesterase 1C is dispensable for rapid response termination of olfactory sensory neurons

Katherine D. Cygnar and Haiqing Zhao

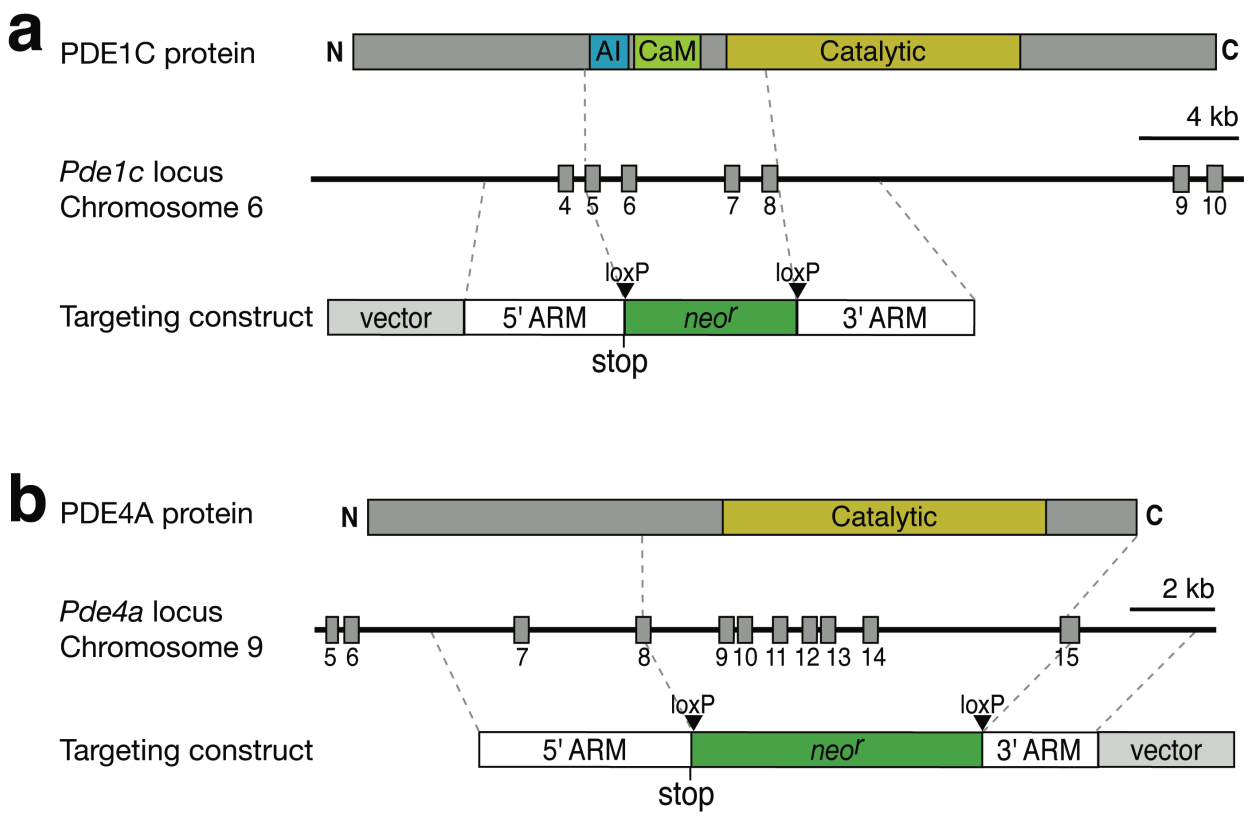

Supplementary Figure 1: Targeting strategy for generation of *Pde1c*$^{-/-}$ and *Pde4a*$^{-/-}$ mice.

(a) Strategy to generate *Pde1c*$^{-/-}$ mice. The PDE1C protein is diagrammed on the top. AI, predicted autoinhibitory domain; CaM, predicted CaM-binding domain; Catalytic, predicted catalytic domain. The *Pde1c* gene is located on chromosome 6 in mice. A portion of the *Pde1c* gene structure and the targeting construct are shown in the middle and the bottom respectively. Exon numbering follows the numbering in the Ensembl database (www.ensembl.org). Homologous recombination with the targeting vector deletes 6.7 kilobases of genomic DNA, including a portion of the catalytic domain, and also inserts a stop codon in exon 5. The vector was constructed from DNA fragments amplified by high fidelity PCR from 129/Sv mouse genomic DNA. The 5' arm was amplified with forward primer 5'–TTGGCAGACAGGATGTTC–3' and reverse primer 5'–CTCTGTATCCAGCAGTCGCCT–3'. The 3' arm was amplified with forward primer 5'–CCAGCTATGATGAGGGTGAGC–3' and reverse primer 5'–GCTGATGAAGCTGTTTGATTC–3'. Restriction sites were added at the end of each primer to facilitate targeting vector construction. A loxP–neo–loxP (LNL) selection cassette (Zhao & Reed, *Cell* **104**, 2001) was included between the two homologous arms. The targeting vector was linearized and electroporated into mouse ES cells (MC1 clone, Johns Hopkins University transgenic facility). The homologous recombination events were screened by PCR of genomic DNA using primer pairs that cross the homologous arms. The modified ES cells were injected into C57BL/6 blastocysts and implanted into pseudopregnant females to generate chimeric offspring. Blastocyst injections were performed at the Johns Hopkins University transgenic

facility. Chimeric males were mated to C57BL/6 females to obtain germline transmission. The LNL fragment was removed from the genome by mating heterozygotes with cre–transgenic mice (Schwenk, Baron, & Rajewsky, *Nucleic Acids Res* **23**, 1995). Knockout mice with and without the LNL cassette were used for experiments and no differences were noted between them.
(b) Strategy to generate *Pde4a*$^{-/-}$ mice. The PDE4A protein is diagrammed on the top with the predicted catalytic domain marked in yellow. The *Pde4a* gene is located on chromosome 9 in mice. A portion of the *Pde4a* gene structure and the targeting construct are shown in the middle and the bottom respectively. Exon numbering follows the Ensembl database. Homologous recombination with the targeting vector deletes 9.9 kilobases of genomic DNA, including the entire predicted catalytic domain, and also inserts a stop codon in exon 8. The vector was constructed from DNA fragments amplified by high fidelity PCR from 129/Sv mouse genomic DNA. The 5' arm was amplified with forward primer 5'–AGAGGTCCTCCTGATCTGTC–3' and reverse primer 5'–GCCAAACCTCCTTTCTCTGTG–3'. The 3' arm was amplified with forward primer 5'–CCTGTGTGAGAGGGACTCGCT–3' and reverse primer 5'–CCTGATCCCTTTTCCCTTCAC–3'. Targeting in ES cells and generation of chimeras was as described for the *Pde1c* knockout.

Supplementary Table 1: Analysis of EOG responses (Heptaldehyde stimulation)

			Wildtype	*Pde1c*$^{-/-}$	*Pde4a*$^{-/-}$	*Pde1c*$^{-/-}$: *Pde4a*$^{-/-}$
Response to Single Pulse	**Maximum amplitude (mV)**		23.0 ± 3.1 (7)	11.8 ± 2.6 (5) **	22.4 ± 2.5 (5)	12.7 ± 3.4 (8) **
	Latency (ms)	10^{-4} M	107.3 ± 3.1 (15)	120.7 ± 7.6 (9) **	108.9 ± 4.6 (14)	118.6 ± 6.0 (17) **
		10^{-3} M	113.5 ± 3.9 (15)	124.7 ± 5.3 (10) **	113.1 ± 4.9 (14)	127.0 ± 4.7 (18) **
		10^{-2} M	85.2 ± 2.1 (15)	100.8 ± 5.7 (10) **	84.6 ± 3.5 (14)	102.7 ± 3.4 (18) **
	Rise time (ms)	10^{-4} M	250 ± 9 (15)	361 ± 37 (10) **	257 ± 10 (14)	399 ± 14 (18) **
		10^{-3} M	276 ± 14 (15)	358 ± 15 (10) **	280 ± 13 (14)	438 ± 20 (18) **
		10^{-2} M	271 ± 18 (15)	386 ± 14 (10) **	281 ± 16 (14)	487 ± 23 (18) **
	Termination τ (s)	10^{-4} M	0.53 ± 0.05 (20)	0.41 ± 0.03 (14) **	0.55 ± 0.07 (14)	1.04 ± 0.08 (17) **
		10^{-3} M	0.91 ± 0.08 (20)	0.70 ± 0.03 (14) **	0.88 ± 0.10 (14)	1.54 ± 0.23 (18) **
		10^{-2} M	1.75 ± 0.19 (20)	1.34 ± 0.14 (13) **	1.89 ± 0.19 (14)	3.54 ± 0.84 (18) **
Adaptation	**Paired-pulse: ratio of 2nd pulse to 1st pulse**	10^{-4} M	0.57 ± 0.03 (13)	0.64 ± 0.03 (9) **	0.53 ± 0.06 (8)	0.47 ± 0.05 (8) **
		10^{-3} M	0.45 ± 0.04 (13)	0.60 ± 0.03 (9) **	0.46 ± 0.05 (8)	0.39 ± 0.05 (8)
		10^{-2} M	0.21 ± 0.03 (13)	0.37 ± 0.02 (8) **	0.22 ± 0.03 (8)	0.23 ± 0.03 (8)
	Sustained pulse: % decline at 10 s	10^{-4} M	74.4 ± 3.0 (15)	72.9 ± 4.4 (10)	75.6 ± 3.3 (8)	52.3 ± 9.3 (9) **
		10^{-3} M	64.3 ± 3.5 (15)	60.1 ± 5.1 (10)	62.7 ± 2.9 (8)	31.0 ± 9.8 (9) **
		10^{-2} M	45.6 ± 3.3 (15)	41.4 ± 5.6 (9)	43.4 ± 6.6 (8)	22.4 ± 13.1 (9) **

Odorant concentrations are for heptaldehyde. For maximum amplitude, values are ± SD; for all others, values are ± 95% CI. The number of mice *(n)* is indicated in parentheses. * indicates $P < 0.05$ in an unpaired t-test compared to wildtype, ** indicates $P < 0.01$.

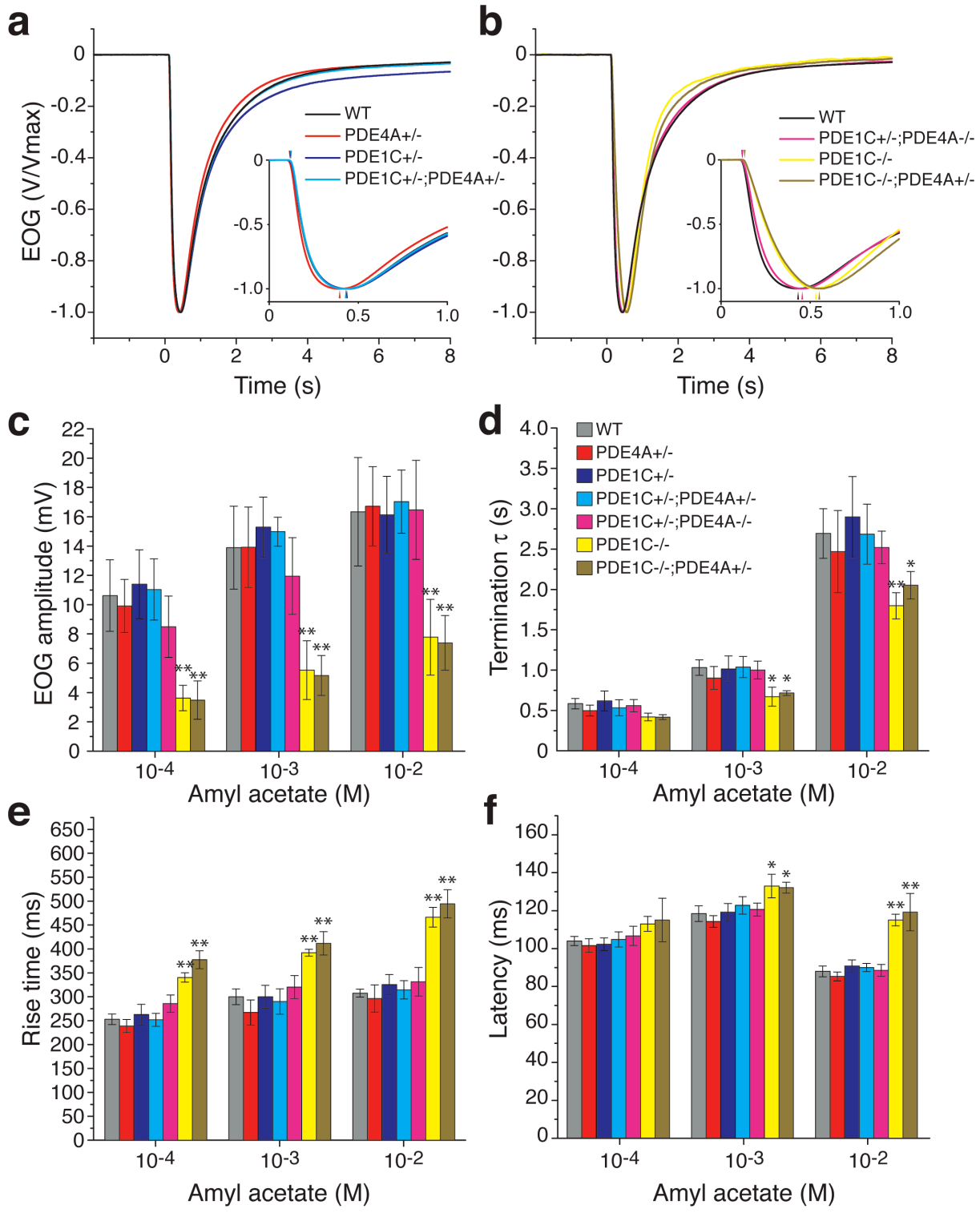

Supplementary Figure 2: EOG responses of heterozygous and compound PDE mutant mice.

(a) Normalized and averaged EOG responses to single 100 ms pulse of 10^{-3} M amyl acetate from wildtype, *Pde4a*$^{+/-}$, *Pde1c*$^{+/-}$, and *Pde1c*$^{+/-}$;*Pde4a*$^{+/-}$ mice. Inset shows the traces plotted on an

expanded time axis. (b) Normalized and averaged EOG responses to the same stimulus as in (a) from *Pde1c*$^{+/-}$;*Pde4a*$^{-/-}$, *Pde1c*$^{-/-}$;*Pde4a*$^{+/-}$, and *Pde1c*$^{-/-}$ mice. Responses of wildtype mice are re-plotted for reference. (c) EOG amplitudes, (d) Termination τ, (e) response rise times, and (f) response latencies. Mice bearing one or two copies of the *Pde1c* gene (*Pde4a*$^{+/-}$, *Pde1c*$^{+/-}$, *Pde1c*$^{+/-}$;*Pde4a*$^{+/-}$, and *Pde1c*$^{+/-}$;*Pde4a*$^{-/-}$) respond similarly to wildtype, and have termination time constants, amplitudes, rise times, and response latencies that are not significantly different from wildtype. *Pde1c*$^{-/-}$;*Pde4a*$^{+/-}$ mice respond similarly to *Pde1c*$^{-/-}$ mice, and have termination time constants, amplitudes, rise times, and response latencies that are significantly different from wildtype but similar to *Pde1c*$^{-/-}$ mice. In (c-f), error bars are 95% CI. All *P* values are from unpaired t-tests following ANOVA. *, $P < 0.05$; **, $P < 0.01$. n= 5 to 6 mice for each genotype.

Supplementary Table 2: Quantification of EOG responses of heterozygous and compound PDE mutant mice.

	Wildtype	*Pde4a*$^{+/-}$	*Pde1c*$^{+/-}$	*Pde1c*$^{+/-}$; *Pde4a*$^{+/-}$	*Pde1c*$^{+/-}$; *Pde4a*$^{-/-}$	*Pde1c*$^{-/-}$	*Pde1c*$^{-/-}$; *Pde4a*$^{+/-}$
Termination τ (s)							
10^{-4} M	0.59 ±0.06	0.50 ±0.07	0.62 ±0.12	0.53 ±0.10	0.56 ±0.08	0.42 ±0.05	0.42 ±0.03
10^{-3} M	1.03 ±0.10	0.90 ±0.14	1.01 ±0.16	1.04 ±0.13	1.00 ±0.11	0.67 ±0.12 *	0.72 ±0.03 *
10^{-2} M	2.69 ±0.31	2.47 ±0.51	2.90 ±0.50	2.68 ±0.37	2.52 ±0.20	1.80 ±0.16 **	2.05 ±0.17 *
Amplitude (mV)							
10^{-4} M	10.6 ±2.4	9.9 ±1.8	11.4 ±2.3	11.0 ±2.1	8.5 ±2.1	3.6 ±0.9 **	3.5 ±1.3 **
10^{-3} M	13.9 ±2.8	13.9 ±2.7	15.3 ±2.1	15.0 ±1.0	11.9 ±2.6	5.5 ±2.0 **	5.2 ±1.4 **
10^{-2} M	16.3 ±3.7	16.7 ±2.7	16.1 ±2.6	17.0 ±2.1	16.5 ±3.4	7.8 ±2.6 **	7.4 ±1.9 **
Rise time (ms)							
10^{-4} M	253 ±11	239 ±14	263 ±22	252 ±14	286 ±18	340 ±10 **	378 ±19 **
10^{-3} M	300 ±16	267 ±26	300 ±24	290 ±27	320 ±24	392 ±7 **	412 ±24 **
10^{-2} M	308 ±8	296 ±28	325 ±21	314 ±19	331 ±30	466 ±21 **	494 ±30 **
Latency (ms)							
10^{-4} M	104 ±2	102 ±4	102 ±3	105 ±4	107 ±5	113 ±4	115 ±11
10^{-3} M	118 ±4	114 ±3	119 ±5	123 ±5	121 ±3	133 ±6 *	132 ±3 *
10^{-2} M	88 ±3	85 ±2	91 ±3	90 ±2	89 ±3	115 ±3 **	119 ±10 **
n	6	5	5	6	5	5	6

Odorant concentrations are for amyl acetate. Values are ± 95% CI. * indicates $P < 0.05$ in an unpaired t-test compared to wildtype, ** indicates $P < 0.01$.

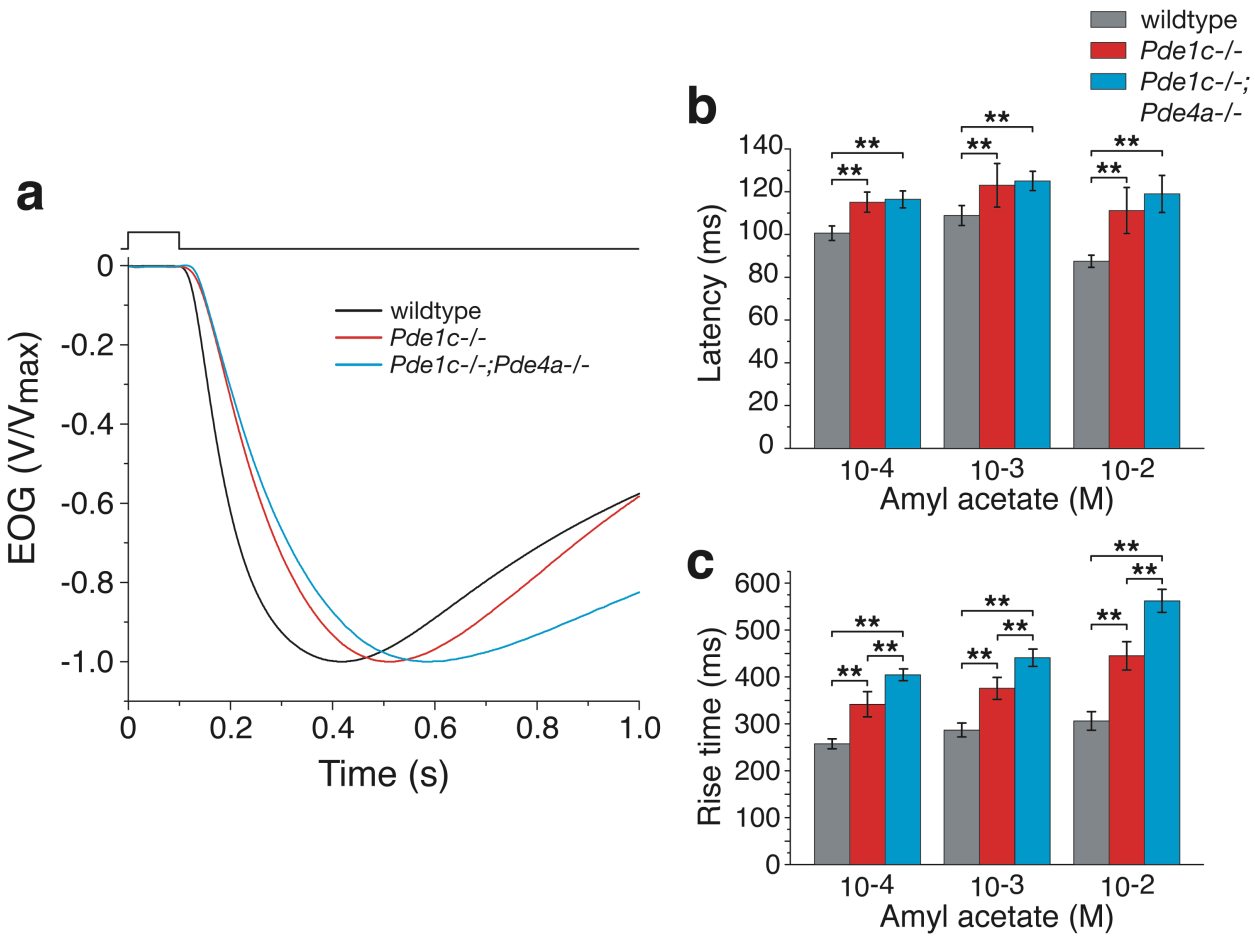

Supplementary Figure 3: *Pde1c*$^{-/-}$;*Pde4a*$^{-/-}$ mice display slower EOG onset kinetics. Data for wildtype and *Pde1c*$^{-/-}$ mice are re-plotted from Fig. 2 for reference. (a) Normalized and averaged EOG responses from *Pde1c*$^{-/-}$;*Pde4a*$^{-/-}$ (n = 17) mice to a single 100 ms pulse of 10^{-3} M amyl acetate, as shown in Fig. 5a, on an expanded time axis. (b) Response latencies. *Pde1c*$^{-/-}$;*Pde4a*$^{-/-}$ mice display significantly longer response latencies compared to wildtype. The longer latencies are comparable to that of *Pde1c*$^{-/-}$ mice. For *Pde1c*$^{-/-}$;*Pde4a*$^{-/-}$ compared to wildtype, $P = 2.0\text{x}10^{-6}$, $3.6\text{x}10^{-5}$, and $4.8\text{x}10^{-7}$ for 10^{-4} M, 10^{-3} M, and 10^{-2} M, respectively. (c) Response rise times. *Pde1c*$^{-/-}$;*Pde4a*$^{-/-}$ mice display response rise times significantly longer than both wildtype mice and *Pde1c*$^{-/-}$ mice. For *Pde1c*$^{-/-}$;*Pde4a*$^{-/-}$ compared to wildtype, $P = 4.0\text{x}10^{-17}$, $2.0\text{x}10^{-13}$, and $6.3\text{x}10^{-16}$ for 10^{-4} M, 10^{-3} M, and 10^{-2} M, respectively. For *Pde1c*$^{-/-}$;*Pde4a*$^{-/-}$ compared to *Pde1c*$^{-/-}$, $P = 8.1\text{x}10^{-5}$, $2.5\text{x}10^{-4}$, and $4.9\text{x}10^{-6}$ for 10^{-4} M, 10^{-3} M, and 10^{-2} M, respectively. For both (b) and (c), error bars are 95% CI. All P values are from unpaired t-tests, n = 17 for *Pde1c*$^{-/-}$;*Pde4a*$^{-/-}$. * indicates $P < 0.05$, ** indicates $P < 0.01$.

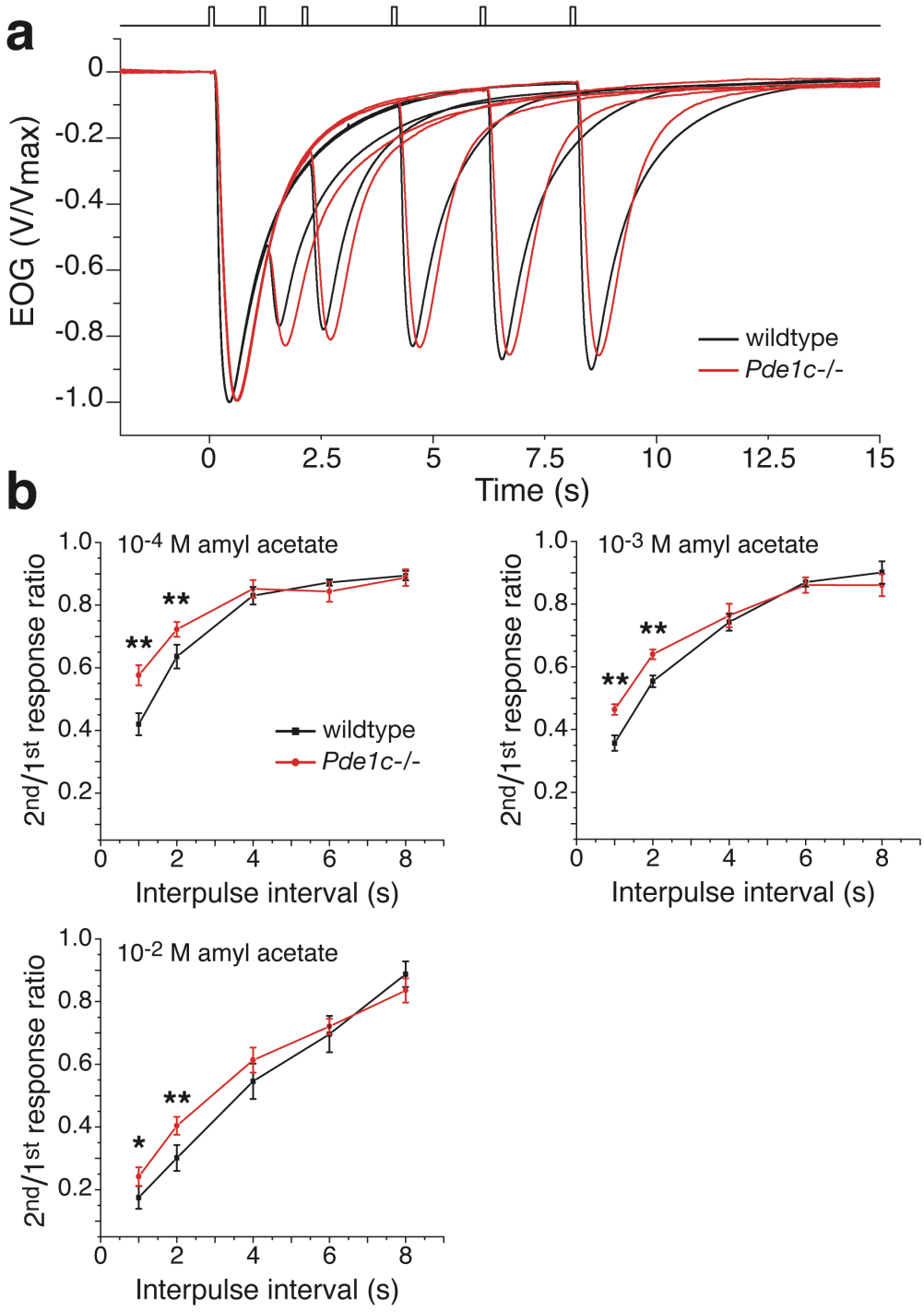

Supplementary Figure 4: Adaptation to repeated stimulation in wildtype and *Pde1c*$^{-/-}$ mice. (a) Normalized and averaged EOG responses to two consecutive 100 ms pulses of 10^{-3} M amyl acetate separated by interpulse intervals of 1, 2, 4, 6, or 8 seconds. (b) Ratio of 2nd net peak amplitude to 1st peak amplitude plotted by the interpulse interval. As the interpulse interval lengthens the response amplitude recovers in both wildtype and *Pde1c*$^{-/-}$ mice, however responses from *Pde1c*$^{-/-}$ mice to the 2nd pulse are significantly larger than wildtype when

interpulse intervals were 1 or 2 seconds. Error bars are SD. For 10^{-4} M amyl acetate, $P = 6.2\text{x}10^{-4}$, 0.0081, 0.32, 0.14, and 0.69 for interpulse intervals of 1, 2, 4, 6, and 8 seconds respectively. For 10^{-3} M amyl acetate, $P = 3.7\text{x}10^{-5}$, $3.0\text{x}10^{-5}$, 0.40, 0.53, and 0.16 for interpulse intervals of 1, 2, 4, 6, and 8 seconds respectively. For 10^{-2} M amyl acetate, $P = 0.029$, 0.0064, 0.098, 0.47, and 0.11 for interpulse intervals of 1, 2, 4, 6, and 8 seconds respectively. All P values are from unpaired t-tests, $n = 4$ for both genotypes. * indicates $P < 0.05$, ** indicates $P < 0.01$.

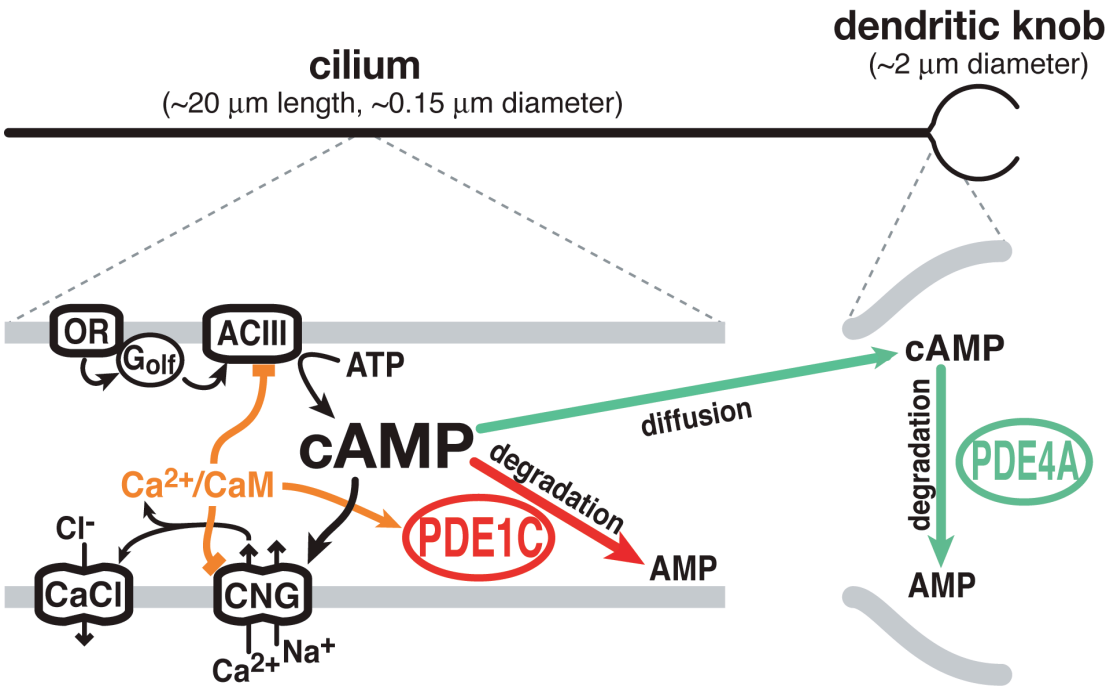

Supplementary Figure 5: Contributions of PDEs to olfactory signal transduction. Odorant stimulation increases the cAMP concentration in the cilia by sequentially activating an odorant receptor (OR), G_{olf}, and ACIII. Increasing levels of cAMP lead to opening of CNG cation channels, allowing influx of Na^+ and Ca^{2+} into the cilia and initiating an electrical signal. The electrical signal is further amplified by opening of Ca^{2+}-activated Cl^- channels (CaCl) and the resulting Cl^- efflux. cAMP removal is achieved by degradation by PDE1C in the cilia and also by diffusion into the dendritic knob and dendrite where it is degraded by PDE4A. In wildtype OSNs, degradation by PDE1C is likely to be the dominant mechanism of cilial cAMP removal while degradation by PDE4A serves as a fail-safe, although both mechanisms may contribute to response termination. When one PDE is absent, the other is sufficient to allow rapid response termination. In the absence of odor stimulation, there is a spontaneous production of cAMP, which is degraded by the basal activity of PDE1C. This dynamic nature of cilial cAMP regulation is likely important in maintaining high sensitivity to odors. Ca^{2+}/CaM stimulates PDE1C activity, which partially accounts for OSN adaptation to repeated stimulation.

Supplementary Note: Computer modeling

We developed a simple model using the Virtual Cell modeling environment (http://www.nrcam.uchc.edu/index.html) to estimate the time course of cAMP diffusion and degradation in the cilia or the dendritic knob. The model is a deterministic 3D spatial model of a single cilium, taken as a cylinder 0.15 μm in diameter[1] and 20 μm in length[2]. The cilium was attached to a "mini-knob" (a sphere with radius 0.43 μm), which has approximately 1/12th the volume of a 2 μm diameter dendritic knob. As many or all cilia would have elevated cAMP levels during odor stimulation, the mini-knob is an estimation of the volume of the dendritic knob that would be available to a single cilium.

We modeled the degradation of cAMP in the cilium and mini-knob, with PDE1C activity restricted to the cilium and PDE4A activity restricted to the mini-knob (Fig. 7b). The cilium was initially filled with 12 μM cAMP, a concentration which saturates the olfactory CNG channels[3]. The degradation of cAMP was modeled in four scenarios: with activities of both PDEs (simulating wildtype); with PDE1C activity only (simulating *Pde4a*$^{-/-}$ OSNs; with PDE4A activity only (simulating *Pde1c*$^{-/-}$ OSNs); and with no PDE activity (simulating double knockout OSNs). The concentrations and activities of PDE1C and PDE4A used in the model and the rationale behind those choices are described below. For all scenarios, cAMP diffusion was set to 270 $\mu m^2 s^{-1}$, the value for cAMP diffusion in OSN cilia determined by Chen et al. (ref. 4).

In the model, cAMP is entirely removed from the cilium within 160 ms when both PDE1C and PDE4A activities are included (wildtype). When PDE1C activity alone is modeled (*Pde4a*$^{-/-}$ OSNs), cAMP is entirely removed only a few milliseconds later. A small amount of cAMP accumulates in the dendritic knob in the model of *Pde4a*$^{-/-}$ OSNs around in the first 140 ms after the start of the simulation, but this concentration peaks at 1.4 μM, a value too low to open a significant portion of CNG channels. This outcome is consistent with the fact that no alterations in the EOG response are observed in *Pde4a*$^{-/-}$ mice.

When only PDE4A activity is modeled (*Pde1c*$^{-/-}$ OSNs), cAMP remains in the cilium for greater than 1 sec, but the concentration remaining is low. At 1 s after the start of the simulation, the highest concentration of cAMP remaining, 3.0 μM, is at the tip of the cilium. The concentration at the base of the cilium is very low at 0.08 μM. This represents an overall much slower rate of cAMP removal compared to when PDE1C activity is included, but this rate is still well within the time course of EOG signal decay, even for very low odorant concentrations. In *Pde1c*$^{-/-}$ OSNs, given the phenotype of reduced sensitivity, this rate of cAMP removal by diffusion with PDE4A degradation is compatible with the faster EOG termination observed, as CNG channels are likely to be desensitized to cAMP and less cAMP may be produced in response to odor.

When neither PDE4A or PDE1C activity is present (the model of *Pde1c*$^{-/-}$*;Pde4a*$^{-/-}$ OSNs), cAMP equilibrates between the cilium and the dendritic knob, producing a severely prolonged elevation of cAMP. In a whole OSN, cAMP would be further diluted in the dendrite and cell body. This extreme extension of cAMP concentrations in the cilia is consistent with the prolonged response termination and increased baseline noise observed in double knockout OSNs.

PDE activity and concentration values

The splice variant of the *Pde1c* gene expressed in OSNs is PDE1C2[5]. The K_m of the PDE1C2 enzyme was determined to be 1.2 μM[6], and this was the value used in the model. No V_{max} data have been published for any variant of PDE1C, although the V_{max} for a related enzyme

PDE1A1 was determined to be 318 μmol min^{-1} mg^{-1} for cGMP[7] in the presence of high Ca^{2+} and CaM, which would translate to a K_{cat} of ~312 s^{-1} assuming a pure preparation of enzyme. Given the high homology between the catalytic domains of PDE1A and PDE1C, PDE1C is also likely to be a very efficient enzyme. We assumed a 2 μM concentration of PDE1C enzyme in the cilia, and set the V_{max} to 100 $\mu M*s^{-1}$ in the model. These parameters produce a time course of degradation of cilia cAMP that approximately matches the degradation of odor-induced cAMP measured in preparations of OSN cilia[8].

The K_m for PDE4A was set to 2.4 μM in the model, which is the K_m reported for the PDE4A5 splice form[9], a PDE4A splice form likely present in the olfactory epithelium (our unpublished data). This value is similar to the 2.0 μM value for the K_m of total PDE activity in olfactory epithelium[10]. The V_{max} for PDE4A is likely much lower than for PDE1C. V_{max} values for different splice forms of purified recombinant human PDE4A expressed either SF9 insect cells [11] or *Saccharomyces cerevisiae*[12] range from 57.5 nmol min^{-1} mg^{-1} to 0.8 μmol min^{-1} mg^{-1}, which would correspond to a K_{cat} of 0.074 to 0.96 s^{-1}. The actual activity of PDE4A in OSNs may be higher than these values, due to regulation of PDE4A activity in the endogenous environment that is not available in heterologous systems. One such regulation is phosphorylation by PKA, which increases the V_{max} of PDE4A from 60%[13] up to 400%[14] depending on the splice form. We assumed a V_{max} of 2 $\mu M*s^{-1}$ to be a reasonable value for PKA-activated PDE4A for the model. The concentration of PDE4A in the dendritic knob was set to 20 μM in the model (given a knob diameter of 2 μm, this would be about 50,000 molecules of PDE4A). With these parameters, when only PDE4A activity is present, the rate of cAMP removal from the cilia approaches the limit set by the diffusion.

References for Supplementary Note

1. Lidow, M.S. & Menco, B.P. Observations on axonemes and membranes of olfactory and respiratory cilia in frogs and rats using tannic acid-supplemented fixation and photographic rotation. *J Ultrastruct Res* **86**, 18-30 (1984).
2. Strotmann, J., Levai, O., Fleischer, J., Schwarzenbacher, K. & Breer, H. Olfactory receptor proteins in axonal processes of chemosensory neurons. *J Neurosci* **24**, 7754-7761 (2004).
3. Song, Y.*, et al*. Olfactory CNG channel desensitization by Ca2+/CaM via the B1b subunit affects response termination but not sensitivity to recurring stimulation. *Neuron* **58**, 374-386 (2008).
4. Chen, C., Nakamura, T. & Koutalos, Y. Cyclic AMP diffusion coefficient in frog olfactory cilia. *Biophys J* **76**, 2861-2867 (1999).
5. Yan, C., Zhao, A.Z., Bentley, J.K. & Beavo, J.A. The calmodulin-dependent phosphodiesterase gene PDE1C encodes several functionally different splice variants in a tissue-specific manner. *J Biol Chem* **271**, 25699-25706 (1996).
6. Yan, C.*, et al*. Molecular cloning and characterization of a calmodulin-dependent phosphodiesterase enriched in olfactory sensory neurons. *Proc Natl Acad Sci U S A* **92**, 9677-9681 (1995).
7. Sonnenburg, W.K.*, et al*. Identification of inhibitory and calmodulin-binding domains of the PDE1A1 and PDE1A2 calmodulin-stimulated cyclic nucleotide phosphodiesterases. *J Biol Chem* **270**, 30989-31000 (1995).
8. Breer, H., Boekhoff, I. & Tareilus, E. Rapid kinetics of second messenger formation in olfactory transduction. *Nature* **345**, 65-68 (1990).

9. McPhee, I., Pooley, L., Lobban, M., Bolger, G. & Houslay, M.D. Identification, characterization and regional distribution in brain of RPDE-6 (RNPDE4A5), a novel splice variant of the PDE4A cyclic AMP phosphodiesterase family. *Biochem J* **310 (Pt 3)**, 965-974 (1995).
10. Borisy, F.F.*, et al*. Calcium/calmodulin-activated phosphodiesterase expressed in olfactory receptor neurons. *J Neurosci* **12**, 915-923 (1992).
11. Wang, P.*, et al*. Expression, purification, and characterization of human cAMP-specific phosphodiesterase (PDE4) subtypes A, B, C, and D. *Biochem Biophys Res Commun* **234**, 320-324 (1997).
12. Wilson, M., Sullivan, M., Brown, N. & Houslay, M.D. Purification, characterization and analysis of rolipram inhibition of a human type-IVA cyclic AMP-specific phosphodiesterase expressed in yeast. *Biochem J* **304 (Pt 2)**, 407-415 (1994).
13. MacKenzie, S.J.*, et al*. Long PDE4 cAMP specific phosphodiesterases are activated by protein kinase A-mediated phosphorylation of a single serine residue in Upstream Conserved Region 1 (UCR1). *Br J Pharmacol* **136**, 421-433 (2002).
14. Laliberte, F.*, et al*. In vitro PKA phosphorylation-mediated human PDE4A4 activation. *FEBS Lett* **512**, 205-208 (2002).